ORGANIC CHEMISTRY

FRONTIERS







View Article Online
View Journal | View Issue

RESEARCH ARTICLE



Cite this: *Org. Chem. Front.*, 2018, **5**, 3170

Pyridine-terminated low gap π -conjugated oligomers: design, synthesis, and photophysical response to protonation and metalation†‡

Asmerom O. Weldeab,^a Lei Li,^a Seda Cekli,^a Khalil A. Abboud,^a Kirk S. Schanze o^{a,b} and Ronald K. Castellano o^x

Reported here is the design and synthesis of among the first pyridine terminated acceptor–donor–acceptor–donor–acceptor–donor–acceptor (A–D–A–D–A) based π -conjugated oligomers, EH_DPP_2T_Pyr (1), EH_II_2T_Pyr (2), and EH_II_1T_Pyr (3). The molecules incorporate thiophenes as electron donors, isoindigo/diketopyr-rolopyrrole as electron acceptors, and are capped with pyridine, a weak electron acceptor, on both ends. All target oligomers show attractive photophysical properties, broad absorption in the visible region (λ_{max} = 636 nm, 575 nm, and 555 nm, for 1, 2, and 3, respectively) and emission which extends to the IR region (emission λ_{max} = 734 nm and 724 for 1 and 2, respectively). Given the pyridine nitrogens, the opto-electronic properties of the compounds can be further tuned by protonation/metalation. All compounds show a bathochromic shift in visible absorption and fluorescence quenching upon addition of trifluoro-acetic acid (TFA). Similar phenomena are observed upon addition of metals with a particularly strong response to Cu²⁺ and Pd²⁺ as indicated by Stern–Volmer analysis (e.g., for Pd²⁺; K_{sv} = 7.2 × 10⁴ M⁻¹ (λ = 673 nm), 8.5 × 10⁴ M⁻¹ (λ = 500 nm), and 1.1 × 10⁵ (λ = 425 nm) for 1, 2, and 3, respectively). The selective association of the molecules to Cu²⁺ and Pd²⁺ is further evidenced by a color change easily observed by eye and under UV light, important for potential use in colorimetric sensing.

Received 5th September 2018, Accepted 30th September 2018 DOI: 10.1039/c8qo00963e

rsc.li/frontiers-organic

Introduction

 π -Conjugated organic molecules are promising synthetic frameworks for the design of various functional materials. Thiophene based oligomers and polymers are among the most widely studied and deployed π -systems owing to their useful electronic, optical, redox, and stability properties as well as stacking preferences in the solid state and on surfaces. Thiophenes, generally recognized as electron-rich heterocycles, additionally marry well with comparably electron-poor *N*-heterocycles (*e.g.*, isoindigo and diketopyrrolopyrrole) to create low optical gap donor–acceptor (D–A) constructs that display unique optical and electronic properties as a conse-

quence of their visible light absorption.⁶⁻⁹ Among the standard N-heterocycles, pyridine possesses a single basic nitrogen atom that upon exposure to Brønsted and Lewis acids, metals, or alkylating agents renders the aromatic even more electron deficient. Consequently, hybrid pyridine-thiophene π -conjugated molecules offer the opportunity for stimulidependent optical tuning that is relevant to molecular switches, memory devices, and sensors. Some thienyl-pyridyl constructs have been fundamentally studied in this regard. 10-18 Reissig and co-workers, for example, have reported several thiophene substituted monopyridine derivatives as well as bipyridine derivatives bridged by thiophene, benzene, or acetylene units which show bathochromic shifts upon protonation using TFA.12,14,15 Similar studies have been reported by Finney and co-workers using alternating 2,5-linked pyridinethiophene oligomers.11 Baxter, et al. have reported several pyridyl-thienyl based macrocycles which are sensitive to both protonation and metalation.¹³ Similar studies have been reported by Bai, et al. and Jin, et al. using fluorescent conjugated polymers for Pd2+ detection. 17,18 Despite these efforts, to the best of our knowledge no low-gap donor-acceptor π -systems, otherwise attractive for a variety of organic optoelectronic applications, 8,19 have been explored with respect to pyridine-based changes in their photophysical behavior.

^aDepartment of Chemistry, University of Florida, Gainesville, FL 32611, USA. E-mail: castellano@chem.ufl.edu; http://www.chem.ufl.edu/~castellano/ ^bDepartment of Chemistry, University of Texas at San Antonio, One UTSA Circle, San Antonio, TX 78249, USA

 $[\]dagger$ Dedicated to Julius Rebek, Jr. on the occasion of his 75th birthday.

 $[\]ddagger$ Electronic supplementary information (ESI) available: Synthetic methods and details, additional absorption and emission data, computational data (energies and coordinates of geometry-minimized structures), copies of 1H / ^{13}C NMR spectra, and details of X-ray data collection and structure refinement. CCDC 1865380. For ESI and crystallographic data in CIF or other electronic format see DOI: 10.1039/c8q000963e

Fig. 1 Chemical structures of the pyridine-terminated donor-acceptor molecules prepared and studied in this work.

Reported here is the design and synthesis of among the first acceptor-donor-acceptor-donor-acceptor (A-D-A-D-A)^{20,21} oligomers featuring terminal pyridyl groups (Fig. 1). The oligomers embed isoindigo (II) or diketopyrrolopyrrole (DPP) acceptors, well-characterized in functional π -systems,⁸ and either mono- or bithiophene spacers. Beyond synthesis, the structural (by computation and X-ray analysis) and solution-phase photophysical properties of the molecules have been studied. The compounds display narrow optical energy gaps, affording strong visible absorption as well as emission extending into the IR region. The structural and photophysical responses of the oligomers to various stimuli (e.g., Brønsted acids, Lewis acids, and/or metals) have also been studied, with significant sensitivity noted (through Stern-Volmer treatments) towards Cu²⁺ and Pd²⁺ ions. Worth noting, these metals, in particular, are significant pollutants due to their use in various chemical and industrial sectors, and their exposure has adverse effects on both plants and animals.22-26

Results and discussion

Synthesis

Shown in Scheme 1 is the synthetic approach to the target compounds EH_DPP_2T_Pyr (1), EH_II_2T_Pyr (2), and EH_II_1T_Pyr (3). Full synthetic details are given in the ESI (Fig. S1at). In all cases, racemic 2-ethylhexyl alkyl chains were installed to enhance solubility. The alkylated DPP core unit (4) was synthesized following literature procedures.27-29 The synthesis of alkylated II core unit (5) also followed literature precedent as provided by Reynolds and coworkers. Both precursors were obtained in comparable yields to the ones reported in the literature.

The synthesis of the stannylated end groups (9, 10) involved multiple steps beginning from commercially available 4-bromopyridine hydrochloride. Compound 6 (see Fig. S1[‡]) was obtained following a literature method³⁰ and was brominated at the alpha-thiophene position using NBS to give 7. The brominated product was exposed to Stille coupling conditions with commercially available 2-(tributylstannyl)thiophene to give 8 in good yield. Both 6 and 8 were then stannylated following a literature method to give 9 and 10, respectively.³¹

Scheme 1 Synthesis of EH_DPP_2T_Pyr (1), EH_II_2T_Pyr (2), and EH_II_1T_Pyr (3). Additional synthetic details and intermediates can be found in the ESI (e.g., Fig. S1‡).

Ultimately, the final target compounds were obtained in average yields using palladium-catalyzed Stille cross-coupling conditions. The products were precipitated by pouring the reaction mixtures into cold acetone to give compound 1 as a dark purple solid, and compounds 2 and 3 as dark brown solids. The structural integrity of the compounds (1-3) was confirmed by 1H NMR, 13C NMR, and high resolution mass spectrometry (HRMS).

Structural analysis

Crystal structure. A crystal of compound 2 was obtained from a 100 µM dilute DMF solution (Fig. 2a-c). Single crystal X-ray analysis shows that the molecule is quite planar which

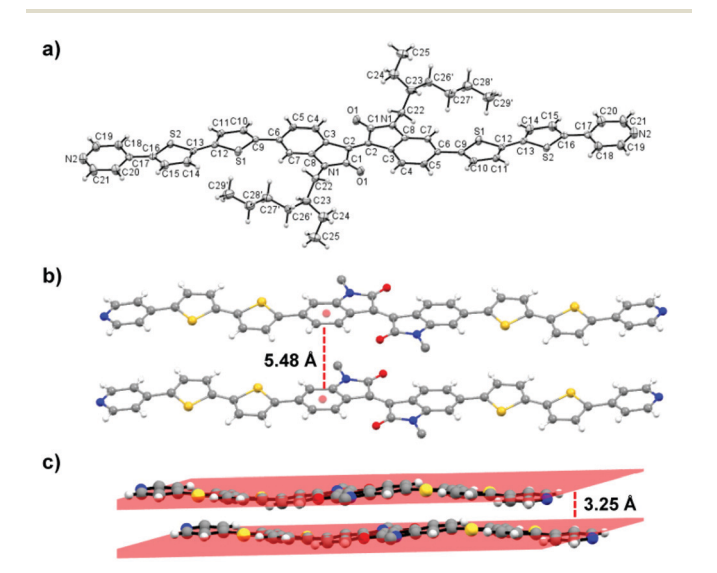


Fig. 2 X-ray crystal structure of compound 2. (a) The full molecule is shown using thermal displacement ellipsoids at 40%. (b) packing diagram showing the distance between adjacent ring centroids, and (c) packing diagram showing the distance between molecular planes (side chain disorder has been removed for clarity in a, and alkyl chains are omitted in (b), (c) for clarity).

maintains its low optical gap. To wit, only a slight twisting is observed between the isoindigo/thiophene (C5–C6–C9–S1 = 8°) and second thiophene/pyridine (S2–C16–C17–C20 = 10°) units; no twisting is noted between the two thiophenes (S1–C12–C13–S2 = 0°). Disorder was observed in the 2-ethylhexyl side chains and could be fully refined in two parts where each has roughly 50% occupancy (see Fig. S2 in the ESI‡ for details). Further analysis indicates that the molecules are packed in a slip stacked herringbone pattern with an interplanar distance of 3.25 Å and intermolecular ring centroid distance (as shown) of 5.48 Å between adjacent slip stacked molecules. Attempts to grow a crystal of compound 1 for direct comparison were not successful.

Calculations. Electronic structure calculations were performed in the gas phase at the B3LYP/6-31G* level of theory to obtain the optimized ground state geometries, orbital energies, and estimated HOMO-LUMO gaps of 1-3 (Fig. 3 and Fig. S3‡). In all cases, the 2-ethylhexyl groups were truncated to methyl groups for simplicity, since they are not expected to affect the equilibrium geometries or electronic properties. For compound 1, the conformation/orientation of the thiophenes with respect to DPP was initially set based on reported crystal structures of similar sytems. 32,33 For 2 and 3, the conformation/orientation of the thiophenes with respect to the core unit (II) was set based on the X-ray crystal structure of 2 (Fig. 2). In all cases the lowest energy conformations obtained from gas phase theoretical calculations (i.e., with respect to the significant dihedral angles) agree with the conformation obtained from the crystal structure (Fig. S4a‡).

The planarity of compound 1 is generally enhanced when compared to 2 and 3 with significant torsion angle difference (20°) at the connection between the core acceptor unit and thiophene (Fig. S4a‡). The planarity of 2 in the gas phase can also be compared to the X-ray crystal structure; planarity is enhanced in the solid state where the torsion angles are each reduced by about 10° compared to the calculated structure (Fig. S4b‡). The overall enhanced planarity speaks to the improved intermolecular overlap in the crystal. With respect to electronic structure, the HOMO energy level of compound 1 (-4.95 eV) is significantly higher than that of compound 2 (-5.21 eV); given that both compounds share similar LUMO energy levels (compound 1 = -2.96 eV, compound 2 = -2.98 eV), this leads to a lower energy gap for 1 ($E_g = 1.99$ eV) when

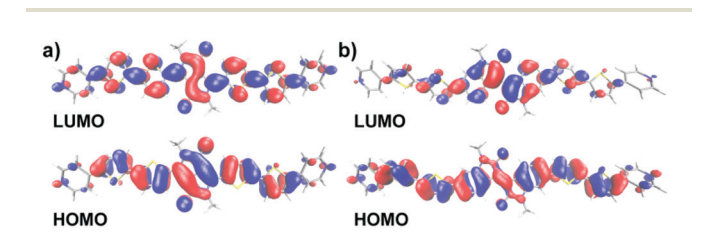


Fig. 3 HOMO (bottom) and LUMO (top) frontier molecular orbital plots of 1 (a) and 2 (b) based on DFT calculations (B3LYP/6-31G*). Gas-phase orbital energies are given in Table 1. 2-Ethylhexyl groups have been truncated to methyl groups for the calculations.

compared to 2 ($E_{\rm g}=2.23$ eV). The low energy gap in 1 is consistent with literature reports where DPP based copolymers showed narrower band gaps compared to their isoindigo based counterparts. The HOMO-LUMO gap of 3 ($E_{\rm g}=2.41$ eV) is larger than the other two which is expected as it possesses fewer thiophene units which reduces the conjugation length of the molecule. The overall trend in energy gap observed among the compounds is consistent with experimental results obtained from UV-Vis (Fig. 4). Frontier molecular orbital plots of compound 1 and 2 are depicted in Fig. 3 (and Fig. S3‡ for compound 3). Unlike compound 1, whose HOMO and LUMO are delocalized throughout the π -system, compounds 2 and 3 show a more significant donor–acceptor structure with the LUMO more localized on the acceptor core unit (II) and the HOMO more localized on the thiophene units.

Photophysical properties

The absorption and fluorescence spectra of 1, 2, and 3 in THF are shown in Fig. 4 and the data is summarized in Table 1. All molecules show strong absorption in the visible region characterized by split high and low energy absorption bands common to donor-acceptor systems (Fig. 4a). Based on previous reports, 34,35 the high energy band is attributed to a localized π - π * transition involving the thienyl-pyridyl portion while the low energy band arises from internal charge transfer. The absorption bands of compound 3 are generally blue shifted (by 46 nm in the high energy band and 20 nm in the low energy band) when compared to 2 due to its shorter conjugation length. The high energy absorption band of the compounds displayed similar features with respect to maximum absorption ($\lambda_{\text{max}} = 381 \text{ nm for } 1, 2 \text{ and } 335 \text{ nm for } 3$); this could be attributed to the end group similarity of the molecules (pyridine-thiophene unit). The low energy charge transfer band of

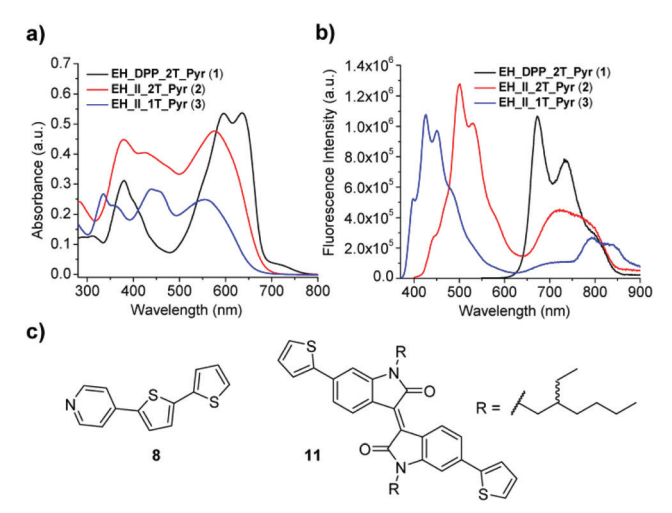


Fig. 4 Absorption (a) and fluorescence (b) spectra of 1, 2, and 3 in THF (10 μ M) (molar extinction coefficient (ϵ) of 1 = 4.8 \times 10⁴ M⁻¹ cm⁻¹, 2 = 3.9 \times 10⁴ M⁻¹ cm⁻¹, and 3 = 2.6 \times 10⁴ M⁻¹ cm⁻¹), (c) chemical structure of end group 8 and core unit 11 used as test compounds. $\lambda_{\text{excitation}}$ of 1 = 390 nm, 2 = 380 nm, and 3 = 355 nm.

Table 1 Summary of optical and electronic properties

	UV-Vis spectroscopy			Pl	DFT calculations ^a		
Compound	λ_{\max} (nm)	$\lambda_{\text{on.}}^{b} (\text{nm})$	$E_{\text{g-opt}}^{c}(\text{eV})$	Fluorescence Em λ_{\max} (nm)	HOMO (eV)	LUMO (eV)	$E_{\rm HL}$ (eV)
1	381, 602, 636	683	1.81	673, 734	-4.95	-2.96	1.99
2	381, 575	678	1.83	501, 530, 724	-5.21	-2.98	2.23
3	335, 439, 555	659	1.88	425, 450	-5.42	-3.01	2.41

^a All 2-ethylhexyl groups have been replaced by methyl groups for the calculations. Geometry optimization and calculation of the HOMO and LUMO energies were performed at the B3LYP/6-31G* level. ^b λ_{onset} was determined by intersection of a tangent through the low energy absorption edge with the abscissa. ^c Determined based on UV absorption data in THF.

compound 1 is structured and slightly red-shifted when compared to the structureless low energy band of 2 and 3 which could be due to the difference in the strength of the acceptor core unit. The narrow optical gap of the molecules determined experimentally from the absorption onset is supported by DFT calculations. As shown in Table 1, an increasing gap is observed going from 2 to 3 which is in agreement with the computational results. The slight redshift observed in the onset of 1 (683 nm) when compared to 2 (678 nm) is also in good agreement with theoretical calculations. Linear Beer–Lambert plots for 1–3 show the molecules are not aggregating in solution within the concentration range used (2.5–20 μ M) (Fig. S5‡).

The fluorescence properties of the compounds were also studied in THF (Fig. 4b). All compounds display an emission band which covers the visible and portion of the near-infrared region. Compound 1 shows a structured emission band with λ_{max} = 673 nm, 734 nm and a Stokes shift of 71 nm. The large Stokes shift observed suggests conformational changes upon excitation of the molecule.36,37 Surprisingly, compounds 2 and 3, which bear the isoindigo acceptor core, show dual fluorescence; a structured high energy band (λ_{max} = 501 nm, 530 nm for 2 and λ_{max} = 425 nm, 450 nm for 3) and structureless low energy band which is more pronounced in 2 (λ_{max} = 724 nm) leading to a very large Stokes shift of 149 nm. We believe the dual fluorescence observed in compounds 2 and 3 is a unique characteristic of the isoindigo core unit. To have more insight into this phenomenon, emission spectra of both the core unit (11) and end group (8) were recorded in THF (Fig. S6‡). Test compound 11 was chosen over 5 (which showed very low fluorescence intensity) and was synthesized following Stille coupling conditions between 5 and 2-(tributylstannyl) thiophene (Fig. S1a[‡]). While 8 exhibits a single fluorescence band, 11 presents dual fluorescence suggesting the origin of the dual fluorescence is from the isoindigo unit. Further studies of this photophysical phenomenon are in progress.

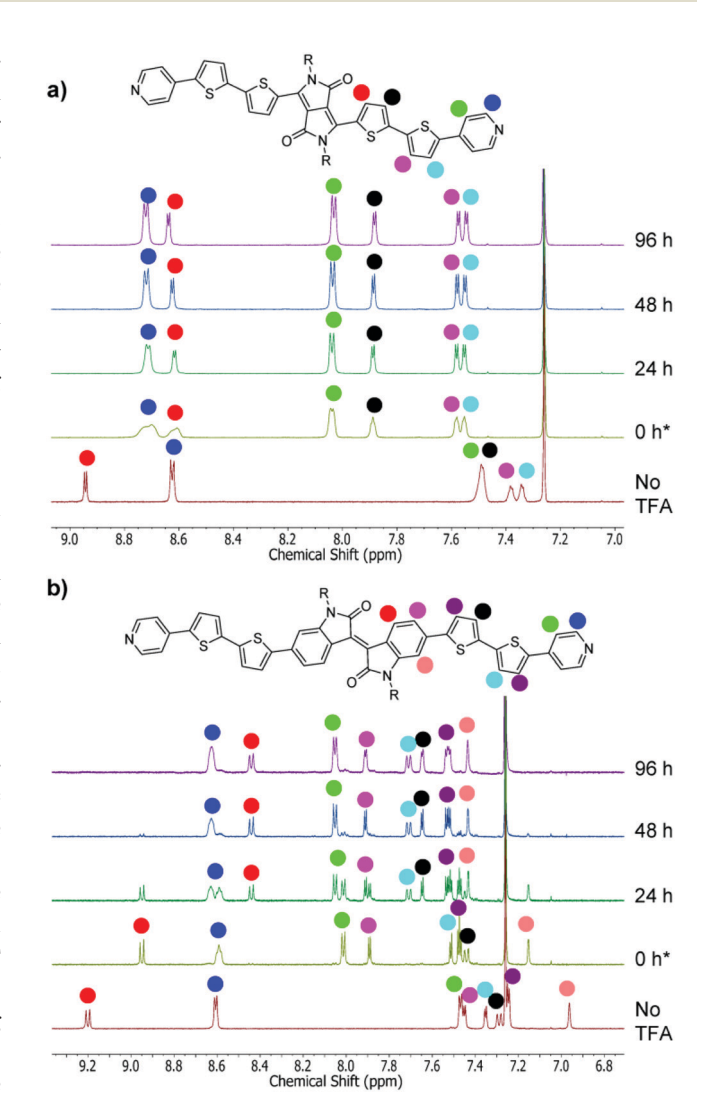


Fig. 5 Variation of the 1 H NMR spectra (aromatic region) of 1 (a) and 2 (b) with time in the presence of 9000 equiv. of TFA in CDCl₃. * = immediately after TFA addition.

Responses to external stimuli

Protonation. Prior to determining the optical response to protonation, the process was examined for 1 and 2 by ¹H NMR in order to confirm the protonation site and stability of the molecules under acidic conditions (Fig. 5a and b). Upon addition of a large excess of trifluoroacetic acid (TFA) to 1 and 2,

all but one of the resonances (indicated by the red circle) shifted downfield. This particular proton, situated closest to the core, shifted upfield in both 1 (by 0.3 ppm) and 2 (by 0.25 ppm). To understand the phenomena, the same ¹H NMR studies were performed using simple DPP/II core units (4/5)

Research Article

and end group 8 (Fig. S7a-c‡). For end group 8, the spin multiplicity of the peak representing the proton alpha to the pyridine nitrogen (indicated by the blue circle) changes from a doublet to a triplet unambiguously confirming protonation of the pyridine (Fig. S7c‡). The same observation is made with 2 (Fig. 5b). But in compound 1, the proton shifts slightly downfield (by 0.09 ppm) and remains a doublet throughout the process which could be due to the difference in pyridine basicity between the compounds. This basicity difference is also reflected in the UV-Vis of the target molecules (Fig. 6) where unlike 2, a large amount of TFA is required to initiate a photophysical response in 1. Coming to the core unit, an upfield shift is observed for the thienyl proton positioned adjacent to the acceptor groups 4 (by 0.45 ppm) and 5 (by 0.27 ppm), consistent with what is observed in the target compounds 1 and 2. This indicates the protonation of the carbonyl oxygen in the lactam ring of the core unit DPP/II which could weaken the electrostatic interaction between this particular proton (indicated with a red circle) and the carbonyl oxygen. A downfield shift is observed in the remaining aromatic protons upon protonation.

No change is observed in the ¹H NMR spectrum of 1 after initial protonation, but compound 2 interestingly shows transformation over several days to a new species. Analyzing the spectra, the shifts observed upon addition of TFA (t = 0 h) are consistent with tri-protonation of the molecules (two pyridine N atoms and one carbonyl O atom). In this tri-protonated state, we believe the proton at the carbonyl undergoes fast exchange on the NMR timescale to give a symmetry-averaged structure. In the case of compound 2, a tetra-protonated state is eventually secured at t ~48 h (Fig. S8‡).

The photophysical response of all the compounds to TFA was then studied by UV-Vis and fluorescence titrations (Fig. 6 and Fig. S9at). Up to 9000 equiv. of TFA was initially used

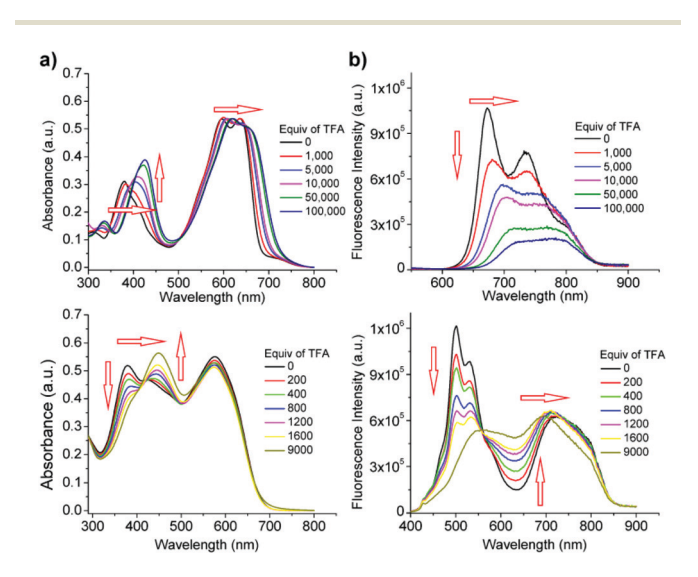


Fig. 6 Absorption (a) and fluorescence (b) spectra generated upon titration of compound 1 (top) and 2 (bottom) with TFA in THF. $\lambda_{\text{excitation}}$ of 1 = 390 nm, and 2 = 380 nm.

based on the amount employed in the NMR experiments. Unlike 2 and 3, only a modest response in the high energy band is observed upon titrating compound 1. Upon introduction of additional equiv of TFA, while no significant change is observed in the low energy band, the high energy absorption band of all compounds red shifts (with increasing intensity). This can be attributed to the reduced optical gap upon protonation at the pyridyl nitrogens, also confirmed by gas phase calculations (Table S9b1). Effectively, the pyridyl acceptors become more electron deficient as true A-D-A-D-A systems are secured.

The fluorescence intensity of compound 1 decreases significantly and the band experiences a bathochromic shift upon increasing the equivalents of TFA (Fig. 6b). The decrease in fluorescence intensity is likely due to excited state proton transfer quenching.13 This facilitates non-radiative decay to the ground state and its effect increases upon increasing the equivalents of TFA. For compound 2, the intensity of the high energy band decreases with the appearance of a newly redshifted band at 590 nm the intensity of which increases upon increasing the equivalents of TFA. A similar phenomenon is observed for compound 3 where the red-shifted band is significantly pronounced (Fig. S9‡). The low energy emission band of 2 and 3 remains unchanged for most of the titration cases (only showing slight quenching at very high concentrations of TFA).

Metalation. The photophysical response of the compounds to metal ions was also studied by fluorescence spectroscopy (Fig. 7). A test was first performed on the DPP containing com-

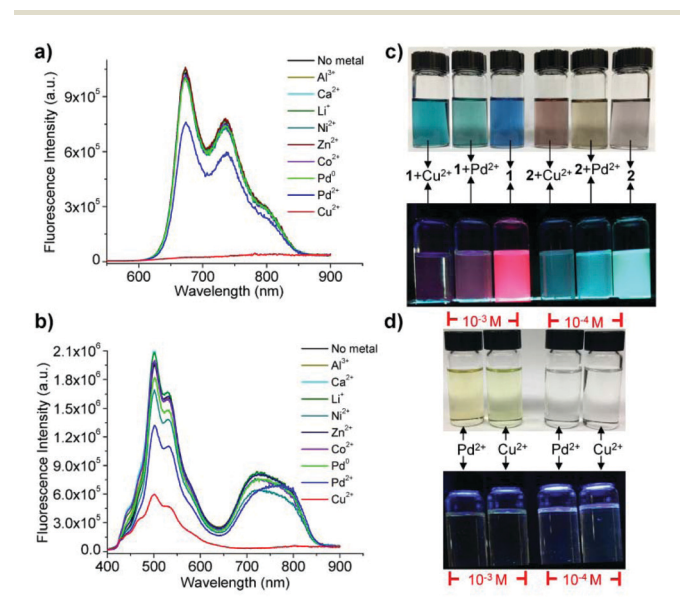


Fig. 7 Fluorescence spectra showing the extent of luminescence quenching of 1 (a) and 2 (b) with 2 equiv. of metal ions. ($\lambda_{\text{excitation}}$ of compound 1 = 390 nm; compound 2 = 380 nm). Photographs which show, (c) color changes of solutions of 1 and 2 upon addition of 10 equiv. (10⁻⁴ M) of Pd^{2+} and Cu^{2+} ; (d) the color of neat Pd^{2+} and Cu^{2+} solutions at different concentrations (10^{-3} M and 10^{-4} M) (for c and d, top pictures: under ambient white light, bottom pictures: with UV lamp (λ = 365 nm) excitation). Metal complexes used: AlCl₃, LiCl, CaCl₂, ZnCl₂, Co(OAc)₂·4H₂O, Ni(OAc)₂·4H₂O, Pd(dba)₂, Pd(OAc)₂, CuCl₂.

pound 1 and one of the II containing compounds 2. Interestingly, when both compounds are exposed to two equivalents of different metal ions (Al3+, Ca2+, Li+, Ni2+, Zn2+, Co²⁺, Pd⁰, Pd²⁺, Cu²⁺) in THF, they show the strongest response to Cu²⁺ and Pd²⁺ (Fig. 7a and b). The fluorescence of 1 is completely quenched upon addition of only two equivalents of Cu²⁺. Similarly, the low energy fluorescence band of 2 is completely quenched with a significant decrease in the high energy band. Substantial quenching is also observed in the intensity of 1 and the high energy fluorescence band of 2 upon addition of two equivalents of Pd2+. Quenching efficiency is generally explained by a combination of two factors: 1. binding affinity for the metal ion to ligand (pyridyl in this case), and 2. intrinsic efficiency for the metal ion to quench the excited state. In our case, the reason Cu2+ and Pd2+ are so efficient is that both ions are very effective excited state quenchers and bind with high stability constant to pyridyl ligands. Cu²⁺ likely quenches by a combination of charge and energy transfer paths, while Pd2+ presumably quenches mainly by heavy atom enhanced singlet to triplet intersystem crossing. The changes in absorption upon addition of Pd2+ and Cu2+ are easily observed by the naked eye and under a UV lamp ($\lambda = 365 \text{ nm}$) which speaks to their potential application as sensors (Fig. 7c and d).

To have more insight into the metal binding efficiency, fluorescence quenching experiments with compounds 1, 2, and 3 were performed in THF (10 µM) using different equivalents of Pd²⁺ (Fig. 8 and Fig. S10[‡]). Indeed, the fluorescence of compound 1 as well as the high energy emission band of compounds 2 and 3 were completely quenched with fewer than 10 equivalents of Pd²⁺. For all compounds the Stern-Volmer plots curved upward (Fig. S11‡) and the Stern-Volmer constants (K_{sv}) were calculated from the linear portion of the curves at low quencher concentrations. All compounds showed strong binding to Pd²⁺ with K_{sv} values of 7.2×10^4 M⁻¹ ($\lambda = 673$ nm), $8.5 \times 10^4 \,\mathrm{M}^{-1}$ ($\lambda = 500 \,\mathrm{nm}$), and $1.1 \times 10^5 \,(\lambda = 425 \,\mathrm{nm})$ for compounds 1, 2, and 3, respectively.

The quenching of the fluorescence could be attributed to the coordination of the metals to the bipyridyl end groups. As proof, the fluorescence properties of test compounds 4/11 (which possess DPP/II core units) and 8 (which possesses pyridine end groups) were separately studied in the presence of Pd²⁺ (Fig. S12[†]). As expected, significant quenching was

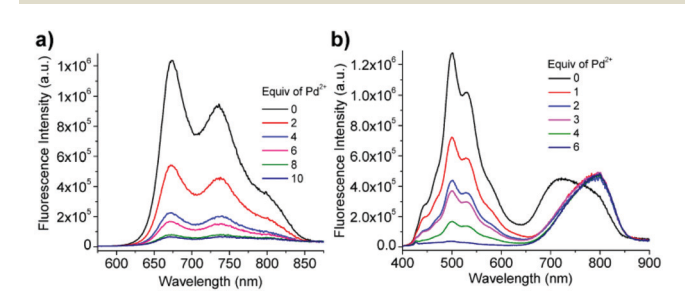


Fig. 8 Fluorescence spectra of 1 (a) and 2 (b) in THF as a function of different equiv of Pd²⁺. $\lambda_{\text{excitation}}$ of **1** = 390 nm, and **2** = 380 nm.

observed when compound 8 was exposed to Pd2+. On the other hand, no change was observed in the emission spectra of compounds 4/11 upon addition of Pd²⁺.

Conclusions

In summary, this work shows the design and synthesis of novel A-D-A-D-A based π -conjugated oligomers bearing a strong internal electron acceptor unit (II or DPP) and terminated with pyridine groups. Gas phase calculations and UV absorption analysis indicate that all molecules possess a narrow HOMO-LUMO energy gap (e.g., 1.8 eV in solution); UV-Vis/fluorescence studies reveal broad absorption/emission in the visible/near IR region for all the compounds which makes them desirable for optoelectronic applications. Incorporation of terminal pyridine units makes the target molecules sensitive to external stimuli, including protons and metals. Each displays a strong photophysical response upon addition of TFA/metal ions as indicated by the bathochromic shift/quenching observed in the UV-Vis/fluorescence spectra. This photophysical response is especially strong upon metalation where selectivity towards Cu²⁺ and Pd²⁺ is observed which is also manifested in a color change easily detected by the naked eye. Overall, these properties make the target molecules attractive for development as colorimetric sensors. Future work will focus on further exploring the photophysical properties of these oligomers and analogues for potential sensing applications. In addition, the future work will address the origin of the dual fluorescence observed in the isoindigo based target molecules.

Experimental section

Synthesis and characterization of target compounds

2,5-Bis(2-ethylhexyl)-3,6-bis(5'-(pyridin-4-yl)-[2,2'-bithiophen]-5-yl)-2,5-dihydropyrrolo[3,4-c] pyrrole-1,4-dione (1). To a 25 mL three-necked round-bottom flask were added 4 (0.11 g, 0.16 mmol), 10 (0.15 g, 0.33 mmol), tetrakis(triphenylphosphine) palladium(0) (37 mg, 0.032 mmol), and anhydrous DMF (8 mL) under argon atmosphere. The mixture was stirred for 18 h at 100 °C. After cooling down to room temperature, the mixture was poured into cold acetone and filtered. The precipitate was further washed with acetone and was dried under vacuum to give a dark purple solid 1 as a mixture of stereoisomers (RR, SS, RS) (54 mg, 0.064 mmol, 40%). ¹H NMR (CDCl₃, 500 MHz): δ 8.94 (2H, d, J = 4.5 Hz), 8.63 (4H, d, J = 5.5 Hz), 7.48 (6H, d, J = 4.0 Hz), 7.37 (2H, d, J = 4.0 Hz), 7.33 (2H, d, J = 4.0 Hz), 4.10-4.01 (4H, m), 1.96-1.90 (2H, m),1.42-1.25 (16H, m), 0.93 (6H, t, J = 7.5 Hz), 0.89 (6H, t, J = 7.5 Hz) 7.0 Hz) ppm; ¹³C NMR (CDCl₃, 125 MHz): 161.5, 150.6, 141.9, 141.5, 140.5, 139.3, 137.8, 136.9, 128.9, 126.5, 126.2, 125.4, 119.6, 108.7, 46.1, 39.5, 30.5, 28.7, 23.9, 23.3, 14.3, 10.7 ppm. HRMS-ESI: m/z [M + H]⁺ calcd for $[C_{48}H_{51}N_4O_2S_4]^+$: 843.2889, found: 843.2847.

Research Article

(E)-1,1'-Bis(2-ethylhexyl)-6,6'-bis(5'-(pyridin-4-yl)-[2,2'-bithiophen]-5-yl)-[3,3'-biindolinylidene]-2,2'-dione (2). Under argon, anhydrous toluene (10 mL) was added to a two-necked roundbottom flask containing 5 (0.10 g, 0.16 mmol), 9 (0.21 g, 0.39 mmol), and tetrakis(triphenylphosphine)palladium(0) (0.040 g, 0.032 mmol). The mixture was heated to 100 °C for 24 h. The reaction mixture was cooled to room temperature and poured into cold acetone. The precipitate obtained was filtered, washed with acetone, and dried under vacuum to give a dark brown solid. The solid was re-dissolved in chloroform, filtered to get rid of any insoluble particles, and evaporated to give a dark brown solid 2 as a mixture of stereoisomers (RR, SS, RS) (85 mg, 0.088 mmol, 55%). ¹H NMR (500 MHz, CDCl₃): δ 9.20 (2H, d, J = 8.5 Hz), 8.61 (4H, d, J = 5.5 Hz), 7.47 (4H, d, J = 5.5 Hz), 7.45 (2H, d, J = 4.0 Hz), 7.36 (2H, d, J = 3.5 Hz), 7.29 (2H, d, J = 8.5 Hz), 7.25 (4H, d, J = 4.0 Hz), 6.96 (2H, s), 3.80-3.68 (4H, m), 1.92-1.90 (2H, m), 1.49-1.34 (16H, m), 1.00 (6H, t, J = 7.5 Hz), 0.94 (6H, t, J = 7.0 Hz) ppm. ¹³C NMR (125 MHz, CDCl₃): δ 168.8, 150.7, 146.0, 143.9, 141.0, 140.2, 139.0, 137.4, 137.2, 132.0, 130.6, 126.3, 125.5, 125.3, 125.2, 121.5, 119.5, 119.1, 105.8, 44.4, 38.1, 31.1, 29.1, 24.6, 23.3, 14.3, 11.0 ppm. HRMS-ESI: m/z [M + H]⁺ calcd for $(C_{58}H_{56}N_4O_2S_4)^+$ calcd: 969.3359, found: 969.3320.

(E)-1,1'-Bis(2-ethylhexyl)-6,6'-bis(5-(pyridin-4-yl)thiophen-2-yl)-[3,3'-biindolinylidene]-2,2'-dione (3). Under argon, anhydrous toluene (10 mL) was added to a two-necked round-bottom flask containing 5 (0.10 g, 0.16 mmol), 10 (0.21 g, 0.47 mmol), and tetrakis(triphenylphosphine)palladium(0) (0.036 g, 0.032 mmol). The mixture was heated to 100 °C for 24 h. The reaction mixture was cooled to room temperature and poured into cold acetone. The precipitate obtained was filtered, washed with acetone, and dried under vacuum to give a dark brown solid. The solid was re-dissolved in chloroform, filtered to get rid of any insoluble particles, and evaporated to give a dark brown solid 3 as a mixture of stereoisomers (RR, SS, RS) (52 mg, 0.064 mmol, 40%). ¹H NMR (500 MHz, CDCl₃): δ 9.20 (2H, d, J = 9.0 Hz), 8.62 (4H, d, J = 6.0 Hz), 7.52 (2H, d, J =4.0 Hz), 7.50 (4H, d, J = 6.0 Hz), 7.43 (2H, d, J = 4.0 Hz), 7.33 (2H, d, J = 9.0 Hz), 6.99 (2H, s), 3.79-3.67 (4H, m), 1.93-1.87(2H, m), 1.48–1.32 (16, m), 0.98 (6H, t, J = 6.5 Hz), 0.93 (6H, t, J = 6.5 Hz)J = 7.0 Hz) ppm. ¹³C NMR (125 MHz, CDCl₃): δ 168.7, 150.7, 146.0, 145.8, 141.5, 141.0, 137.2, 132.3, 130.6, 126.7, 125.6, 121.8, 119.7, 119.5, 105.1, 44.3, 38.0, 31.0, 29.0, 24.4, 23.3, 14.3, 11.0 ppm. HRMS-ESI: m/z [M + H]⁺ calcd for $(C_{50}H_{52}N_4O_2S_2)^+$ calcd: 805.3604, found: 805.3607.

Conflicts of interest

The authors have no conflicts to declare.

Acknowledgements

R. K. C., A. O. W., and L. L. are grateful for financial support the National Science Foundation

CHE-1507561). K. S. S. acknowledges the National Science Foundation (Grant No. CHE-1504727) for support. K. A. A. wishes to acknowledge the National Science Foundation (Grant No. CHE-0821346) and the University of Florida for funding of the purchase of the X-ray equipment. The authors acknowledge University of Florida Research Computing for providing computational resources and support that have contributed to the research results reported in this publication. URL: http://researchcomputing.ufl.edu.

Notes and references

- 1 L. Dou, Y. Liu, Z. Hong, G. Li and Y. Yang, Chem. Rev., 2015, 115, 12633.
- 2 I. Osaka and R. D. McCullough, Acc. Chem. Res., 2008, 41, 1202.
- 3 F. Zhang, D. Wu, Y. Xu and X. Feng, J. Mater. Chem., 2011, 21, 17590.
- 4 I. F. Perepichka, D. F. Perepichka, H. Mengand and F. Wudl, Adv. Mater., 2005, 17, 2281.
- 5 A. Mishra, C. Ma and P. Bäuerle, Chem. Rev., 2009, 109, 1141.
- 6 C. Grand, S. Baek, T. H. Lai, N. Deb, W. Zajaczkowski, R. Stalder, K. Müllen, W. Pisula, D. G. Bucknall, F. So and J. R. Reynolds, Macromolecules, 2016, 49, 4008.
- 7 J. Mei, K. R. Graham, R. Stalder and J. R. Reynolds, Org. Lett., 2010, 12, 660.
- 8 J. D. Yuen and F. Wudl, *Energy Environ. Sci.*, 2013, **6**, 392.
- 9 A. Tang, C. Zhan, J. Yao and E. Zhou, Adv. Mater., 2017, 29,
- 10 J. Zhang, J. Chen, B. Xu, L. Wang, S. Ma, Y. Dong, B. Li, L. Ye and W. Tian, Chem. Commun., 2013, 49, 3878.
- 11 S. V. Rocha and N. S. Finney, Org. Lett., 2010, 12, 2598.
- 12 S. L. Gholap, P. Hommes, K. Neuthe and H. U. Reissig, Org. Lett., 2013, 15, 318.
- 13 P. N. W. Baxter, J. Org. Chem., 2004, 69, 1813.
- 14 M. K. Bera, S. L. Gholap, P. Hommes, K. Neuthe, D. Trawny, J. P. Rabe, D. Lentz, R. Zimmer and H. U. Reissig, Adv. Synth. Catal., 2013, 355, 3463.
- 15 M. K. Bera, P. Hommes and H. U. Reissig, *Chem.*, 2011, 17, 11838.
- 16 D. Trawny, V. Kunz and H. U. Reissig, Eur. J. Org. Chem.,
- 17 H. Huang, K. Wang, W. Tan, D. An, X. Yang, S. Huang, Q. Zhai, L. Zhou and Y. Jin, Angew. Chem., Int. Ed., 2004, 43, 5635.
- 18 B. Liu, Y. Bao, F. Du, H. Wang, J. Tian and R. Bai, Chem. Commun., 2011, 47, 1731.
- 19 M. Más-Montoya and R. A. Janssen, Adv. Funct. Mater., 2017, 27, 1605779.
- 20 S. Steinberger, A. Mishra, E. Reinold, E. Mena-Osteritz, H. Müller, C. Uhrich, M. Pfeiffer and P. Bäuerle, J. Mater. Chem., 2012, 22, 2701.

- 21 S. Steinberger, A. Mishra, E. Reinold, C. M. Müller, C. Uhrich, M. Pfeiffer and P. Bäuerle, Org. Lett., 2011, 13, 90.
- 22 J. Le Bars, U. Specht, J. S. Bradley and D. G. Blackmond, *Langmuir*, 1999, **15**, 7621.
- 23 M. Lafrance and K. Fagnou, J. Am. Chem. Soc., 2006, 128, 16496.
- 24 T. Iwasawa, M. Tokunaga, Y. Obora and Y. Tsuji, *J. Am. Chem. Soc.*, 2004, **126**, 6554.
- 25 C. A. Flemming and J. T. Trevors, *Water, Air, Soil Pollut.*, 1989, 44, 143.
- 26 S. E. Allen, R. R. Walvoord, R. Padilla-Salinas and M. C. Kozlowski, *Chem. Rev.*, 2013, **113**, 6234.
- 27 R. B. Zerdan, N. T. Shewmon, Y. Zhu, J. P. Mudrick, K. J. Chesney, J. Xue and R. K. Castellano, *Adv. Funct. Mater.*, 2014, 24, 5993.
- 28 A. B. Tamayo, M. Tantiwiwat, B. Walker and T. Q. Nguyen, *J. Phys. Chem. C*, 2008, **112**, 15543.
- 29 J. R. Matthews, W. Niu, A. Tandia, A. L. Wallace, J. Hu, W. Y. Lee, G. Giri, S. C. B. Mannsfeld, Y. Xie, S. Cai, H. H. Fong, Z. Bao and M. He, *Chem. Mater.*, 2013, 25, 782.

- 30 J. Wilson, J. S. Dal Williams, C. Petkovsek, P. Reves, J. W. Jurss, N. I. Hammer, G. S. Tschumper and D. L. Watkins, RSC Adv., 2015, 5, 82544.
- 31 E. C. Constable, C. E. Housecroft, M. Neuburger and C. X. Schmitt, *Polyhedron*, 2006, 25, 1844.
- 32 C. Huang, S. Wu, Y. Huang, Y. Chen, S. Chang, T. Wu, K. Wu, W. Chuang and C. Wang, *Chem. Mater.*, 2016, 28, 5175.
- 33 M. A. Naik, N. Venkatramaiah, C. Kanimozhi and S. Patil, J. Phys. Chem. C, 2012, 116, 26128.
- 34 R. Stalder, J. Mei and J. R. Reynolds, *Macromolecules*, 2010, 43, 8348.
- 35 S. Goswami, M. K. Gish, J. Wang, R. W. Winkel, J. M. Papanikolas and K. S. Schanze, ACS Appl. Mater. Interfaces, 2015, 7, 26828.
- 36 R. R. San Juan, A. Payne, G. C. Welch and A. Eftaiha, *Dyes Pigm.*, 2016, **132**, 369.
- 37 B. Souharce, C. J. Kudla, M. Forster, J. Steiger, R. Anselmann, H. Thiem and U. Scherf, *Macromol. Rapid Commun.*, 2009, **30**, 1258.